Polygonal Shapes Reconstruction from Acoustic Echoes Using a Mobile Sensor and Beamforming

Othmane-Latif Ouabi
IRL 2958 Georgia Tech-CNRS
Metz, France
oouabi@georgiatech-metz.fr

Jiawei Yi
Georgia Institute of Technology
Atlanta, GA 30332-0250, USA
jyi@georgiatech-metz.fr

Neil Zeghidour
Google Research, Brain team
Paris, France
neilz@google.com

Nico F. Declercq
Georgia Institute of Technology
Atlanta, GA 30332-0250, USA
declercq@gatech.edu

Matthieu Geist
Google Research, Brain team
Paris, France
mfgeist@google.com

Cédric Pradalier
IRL 2958 Georgia Tech-CNRS
Metz, France
cedricp@georgiatech-metz.fr

***Abstract*—Mapping a structure, such as a metal plate in a ship hull, using acoustic echoes typically requires making assumptions on its shape (e.g. rectangular). This work introduces a more general approach based on beamforming to recover the geometry of arbitrary polygonal-shaped bounded areas from acoustic reflections. Our method only requires a single omni-directional emitter-receiver acoustic device mounted on a mobile platform. We apply beamforming to the acoustic measurements in the geometrical boundary space. We subsequently retrieve the edges from the beamforming results via the minimization of a regularized cost criterion, using a simulated annealing optimizer. We also design a boundary rejection criterion so that their exact number can be recovered based only on a specified upper bound. We assess our method on different geometries in a simulation environment and a real-world setting using ultrasonic guided waves measurements. The results demonstrate that it is efficient for achieving the targeted objectives.**

***Index Terms*—mapping, acoustic echoes, beamforming**

I. Introduction

Acoustic mapping from echoes is a significant challenge that can enable a wide variety of applications, in particular in robotics. When an acoustic wave is emitted by an embedded transmitter, it can propagate in all directions around the emitter. It can be reflected by environmental features (such as the walls of an enclosed space, for instance). Simultaneously, co-located with the emitter, a receiver can receive the acoustic echoes. With such a setup, one objective is the localization of the acoustic reflectors using the measurements acquired along the robot trajectory. For instance, room shape reconstruction in an indoor environment can be made possible using a single mobile unit [2]. More generally, acoustic Simultaneous Localization and Mapping (SLAM) [3], [4] can be achieved to additionally recover the acquisition positions. Another use case is localization and mapping based on Ultrasonic Guided Waves (UWGs) on a large structure such as a ship hull, where the ultrasonic echoes originate from reflections, on the individual plate boundaries, of the wave propagating in the material [1], [5]. These examples are all instances of the "structure from sound (and motion)" problem.

This work is part of the BugWright2 project. This project is supported by the European Commission under grant agreement 871260 - BugWright2.

While acoustic localization and mapping using sensor arrays receive sustained attention in the literature [6], [7], the use of a single omnidirectional sensor remains a challenging task for practical implementation. Indeed, as the measurements contain several first-order as well as high-order echoes, acoustic localization and mapping necessitate echo-detection, identification and association methodologies that are challenging to establish for reverberant and noisy environments [8].

Acoustic echoes in the air have been used to recover a room shape from wall reflections [9], or to achieve acoustic SLAM [3], [4]. However, these works are only tested in simulation. They rely on essential assumptions, such as only first-order echoes are being detected, the echo-wall association is being flawlessly known, or the number of walls to recover is being known a priori. Due to noisy measurements, these assumptions may not always hold for a real-world scenario.

Recent works in the literature focus on acoustic SLAM using Ultrasonic Guided Waves (UGWs) that can propagate over large distances inside materials. In [5], an online approach is designed to simultaneously recover the geometry of individual metal plates while localizing a mobile sensor, but it lacks robustness w.r.t. to detection errors. A second work [1] achieves acoustic SLAM by relying on beamforming [10]. This approach shows promising results, as it does not necessitate explicit echo retrieval and association prone to errors. It has been subsequently improved in [11] through the combination of beamforming and a probabilistic grid representation that builds on the estimation of the first acoustic echo to limit beamforming errors due to interference. However, the beamforming approach for mapping the plate boundaries is limited to rectangular geometries.

The objective of this work is to generalize the approach presented in [1] and [11] to recover arbitrary 2-dimensional polygonal geometries from acoustic echoes. It relies on beamforming in the geometrical boundary space and the *single* detection of the closest boundary to map the inner surface of the

geometric shape. The geometry estimate is then constructed via the minimization of a regularized cost function using a simulated annealing optimizer to select boundaries, on the beamforming results, that are consistent with the mapped inner space. We also design a boundary rejection criterion to recover their exact number based only on a specified upper bound. We test our approach in simulation for various geometries and actual conditions using experimental ultrasonic measurements acquired on a metal plate sample. The results show that it can successfully recover the geometric shape of the reverberant environment, the exact number of boundaries, and has the same performance as the baseline method in [1] for recovering rectangular shapes.

II. Method

We consider a setup where a single (collocated) emitter/receiver acoustic device is driven to acquire acoustic measurements $z_{1..T}(t)$ at positions $\mathbf{x}_{1..T}$ in a delimited space, where $\mathbf{x}_i = [x_i, y_i]^T$ contains the two-dimensional position. At the i-th scanning position, a pulse $s(t)$ is used to emit an omnidirectional acoustic wave. The received signal $z_i(t)$ contains the reflections of the incident wave on the environment boundaries. We assume that noise-free odometry information (*i.e* linear and rotational displacement between the positions of the successive measurements) is available. For a robotic application, it is typically provided by the wheels encoders, but other systems such as an Inertial Measurement Unit (IMU) can also be integrated for better accuracy. We also assume that, at each position $\mathbf{x}_i$, an accurate measurement (or estimate) of the range ρ_i to the closest boundary is available by processing the acoustic data. This measurement may only be subject to little noise in practice, as it may be one of the most energetic echoes. Based on all range measurements $\rho_{1..T}$, the surface A_T is defined as the unions of all disks centered at sensor positions $\mathbf{x}_i$, and whose radius equal to the detected range ρ_i. By construction, this area cannot be crossed by a boundary. The objective is to estimate the shape of the environment $\mathbf{M}$ that we assume to be a 2D convex polygon using measurements and odometry. It should be noted that only the mapping problem is addressed here. Still, the proposed approach is expected to integrate seamlessly within the SLAM framework in [1] to account for odometry noise, and the method in [11] to consider detection errors on the range measurements ρ_i.

A. Measurement model

The acoustic measurements contain successive reflections of the excitation on the boundaries. Under the assumption that the propagation is linear, and the medium is homogeneous and isotropic, we can use the image source model [12]:

$$z_i(t) = \sum_{\mathbf{p}_{i,j} \in \mathcal{I}(\mathbf{x}_i, \mathbf{M})} g(||\mathbf{p}_{i,j} - \mathbf{x}_i||, t) * s(t) + n_i(t), \quad (1)$$

where g is the acoustic transfer function of the isotropic medium, $\mathcal{I}(\mathbf{x}_i, \mathbf{M})$ is the set of image source positions for a real source in $\mathbf{x}_i$, and n_i is additive Gaussian noise that we assume to be spatially and temporally white.

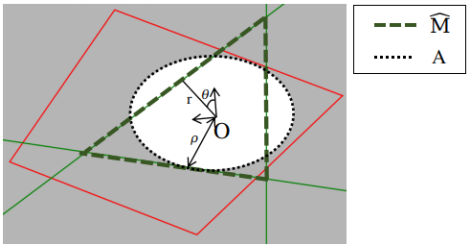

Fig. 1: Schematic of the problem setup and notations. An example of shape to estimate is represented by the red polygon. A candidate geometry estimate is represented by the set of green lines, whose (r, θ) coordinates are only provided for one of them. The area A formed with a single range measurement ρ is represented by the lighter area. The inner surfaces of A and $\hat{\mathbf{M}}$ are delimited with the discontinuous dashed lines.

B. Delay and sum beamforming

The geometry $\mathbf{M}$ to estimate is assumed to be a 2D convex polygon that can be represented by its linear boundaries: $\mathbf{M} = \{r_l, \theta_l\}_{l=1..L}$ where the parameters (r_l, θ_l) define the line equation in the 2D plane with:

$$x \cdot \cos\theta_l + y \cdot \sin\theta_l - r_l = 0, \quad (2)$$

expressed in a fixed frame whose origin will be chosen as the initial robot position, and the x axis will be aligned with the initial robot heading. The number L of boundaries is assumed a priori unknown. The adopted notations are precised in Fig.1. To estimate the map $\mathbf{M}$, we rely on beamforming as in previous works [1]. The approach is recalled here for completeness. We first evaluate the correlation measurements:

$$\tilde{z}_i(r) = \frac{\langle z_i(t), \hat{z}(r,t) \rangle}{\sqrt{\langle z_i(t), z_i(t) \rangle \langle \hat{z}(r,t), \hat{z}(r,t) \rangle}}, \quad (3)$$

where $\hat{z}(r,t) = \hat{g}(2r,t) * s(t)$ is the expected received echo signal for a boundary situated at a distance r from the receiver, and $\hat{g}$ is a model of the transfer function as in [1]. We then retrieve the envelope: $e_i(r) = |\tilde{z}_i(r) + j\mathcal{H}(\tilde{z}_i)(r)|$, where $\mathcal{H}$ denotes the Hilbert transform operator. Hence, the positions of the local maxima of e_i yield the distances to the boundaries, and ρ_i can be selected as the smallest one.

Next, we assess the likelihood of existence for any line boundary (r, θ) by constructing the beamforming map based on the correlation measurements and sensor positions:

$$\mathcal{L}_T(r, \theta) = \sum_{i=1}^{T} e_i \left(d_i(r, \theta) \right), \quad (4)$$

where $d_i(r, \theta) = |x_i \cdot \cos\theta + y_i \cdot \sin\theta - r|$ is the distance between the receiver and the considered line. It is to be noted that only first-order reflections are considered in the above equation, as we reason on individual lines.

C. Spatially-regularized cost function

The previous mapping approach in [1] can only be used to recover rectangular shapes by retrieving exactly four local maxima of $\mathcal{L}_T$ through the maximization of their cumulative

likelihood. We propose to extend this approach to recover, in principle, arbitrary 2D polygonal shapes. The estimated geometry has the form: $\hat{\mathbf{M}} = \{\hat{r}_k, \hat{\theta}_k\}_{k=1..K}$, where the maximum number of boundaries K is such that $K \geq L$. This is a very minimal hypothesis, as K can be set much higher than the unknown L.

Next, for a given robot trajectory $\mathbf{x}_{1..T}$, we determine the inner surface A_T using the measurements $\rho_{1..T}$. Based on the beamforming map $\mathcal{L}_T$ calculated with Eq. (4) that we normalize by its maximum value, we consider the cost:

$$c(\hat{\mathbf{M}}) = -\left(\sum_{(r_k,\theta_k)\in\hat{\mathbf{M}}} \mathcal{L}_T(r_k,\theta_k) + \lambda \frac{\hat{\mathbf{M}} \bigcap A_T}{\hat{\mathbf{M}} \bigcup A_T} \right), \quad (5)$$

where the first term aggregates the likelihood of presence of the estimated boundaries, and the second term is the well known Intersection over Union (IoU), widely used for computer vision purposes [13]. In Eq. (5) the surfaces $\hat{\mathbf{M}}$ and A_T are as described in Fig.1. The IoU term (that we will simply write as $\text{IoU}(\hat{\mathbf{M}}, A_T)$) is always between 0 and 1. It is zero when $\hat{\mathbf{M}}$ and A_T have an empty intersection, and it is 1 when the two surfaces are equal. λ is a positive parameter that balances the importance between the boundaries likelihood and IoU terms. Our geometry estimate is then defined as:

$$\hat{\mathbf{M}}_T = \arg\min_{\hat{\mathbf{M}}} c(\hat{\mathbf{M}}). \quad (6)$$

Hence, the minimization of the cost criterion leads to maximization of the cumulative likelihood of the estimated boundaries and maintains consistency between the estimated inner surface of $\hat{\mathbf{M}}$ with that of A_T. In other words, the IoU in Eq. (5) acts as a regularization term for selecting likely boundaries on the beamforming results.

D. Shape estimation with simulated annealing

An optimization strategy is required to recover a geometry estimate by minimizing the cost. Simulated annealing (SA) [14] is a relatively simple and efficient approach for estimating a global minimum of a non-linear cost function. This metaheuristic is inspired by metallurgy, where, to form a perfect crystal (which corresponds to the state of minimal energy), a pure liquid substance is slowly cooled. A random perturbation is applied to the current state at each iteration of the optimization process. The perturbation is systematically accepted if the energy is decreased. It is accepted according to a Boltzmann probability distribution when the energy is increased to escape local minima. The temperature, which is a hyperparameter that controls the acceptance rate, is decreased slightly after each iteration, so that the probability of increasing the energy goes to zero. Even though simulated annealing offers no guarantees that the optimum will be found, this strategy can lead to satisfying solutions in a relatively restricted number of iterations. In the following, we detail the different steps of our custom implementation for mapping arbitrary polygonal geometries from acoustic echoes.

1) Initialization: First, the geometry estimate is randomly initialized with $\hat{\mathbf{M}}_T = \{\hat{r}_k, \hat{\theta}_k\}_{k=1..K}$, where the $\hat{r}_k$ and $\hat{\theta}_k$ are sampled from independent uniform distributions.

2) State disturbance: At iteration p of the optimization process, each boundary of the estimate is iteratively disturbed with a random process. For the k-th boundary, we sample:

$$\begin{cases} \tilde{r}_k = \max(\hat{r}_k + \Delta_r \cdot \chi_r^3, 0) \\ \tilde{\theta}_k = \hat{\theta}_k + \Delta\theta \cdot \chi_\theta^3 \bmod 2\pi \end{cases}, \quad (7)$$

where Δ_r and Δ_θ are positive parameters, and χ_r and χ_θ are independently sampled from uniform distributions: $\mathcal{U}([-1,1])$. They are raised to the power 3 so that small variations are more likely. Still, large variations (*i.e* in the order of Δ_r and Δ_θ) can be possible to explore regions of the search space that are far occasionally from the current state. Furthermore, to speed up the optimizer convergence, we determine:

$$(\tilde{r}_k, \tilde{\theta}_k) \leftarrow \arg\max_{(r,\theta)\in V(\tilde{r}_k,\tilde{\theta}_k)} \mathcal{L}_T(r,\theta), \quad (8)$$

where $V(\tilde{r}_k, \tilde{\theta}_k)$ denotes the set of boundaries that lie in the neighborhood of $(\tilde{r}_k, \tilde{\theta}_k)$ that is to be appropriately defined. The purpose of this step is to only select $(\tilde{r}_k, \tilde{\theta}_k)$ that are local maxima, which is a property that is expected for the true boundaries. The former edge $(\hat{r}_k, \hat{\theta}_k)$ in $\hat{\mathbf{M}}_T$ is then substituted to the sampled one, yielding a new geometry $\widetilde{\mathbf{M}}_T$.

3) Simulated annealing acceptance process: The new candidate map is kept as the current state following an SA acceptance process. First, we determine the cost variation $\Delta c = c(\widetilde{\mathbf{M}}_T) - c(\hat{\mathbf{M}}_T)$. Let's χ be a sample from $\mathcal{U}([0,1])$. The candidate geometry is kept only if we have:

$$\chi < \exp\left(-\frac{\Delta c}{T(p)}\right), \quad (9)$$

where $T(p)$ is the temperature at iteration p of the optimizer. Hence, if the cost is decreased, the new map is systematically kept as the new current state $\hat{\mathbf{M}}_T$. Otherwise, it is kept according to the Boltzmann distribution to escape local minima.

4) Edge filtering: As it is expected that the edges number parameter K is overestimated, some of them may not contribute significantly to the definition of the recovered geometry once the optimizer has converged. To derive a proper geometry with a correct number of boundaries, we apply a rejection criterion to remove non-informative edges. We iterate over each boundary $(\hat{r}_k, \hat{\theta}_k)$ in $\hat{\mathbf{M}}_T$, and we remove it to yield a new candidate geometry $\widetilde{\mathbf{M}}_T$. We then assess whether:

$$\left| \frac{\text{IoU}(\widetilde{\mathbf{M}}_T, A_T) - \text{IoU}(\hat{\mathbf{M}}_T, A_T)}{\text{IoU}(\hat{\mathbf{M}}_T, A_T)} \right| < \epsilon, \quad (10)$$

where we will take $\epsilon = 10^{-2}$. If the IoU variation is lower than the threshold, then the k-th boundary can be removed, as its contribution to the definition of the geometric surface is considered negligible. Then, the geometry $\widetilde{\mathbf{M}}_T$ can be taken as the new candidate $\hat{\mathbf{M}}_T$, and the process is iterated on the next boundary. Also, the rejection criterion is not applied if the candidate map $\hat{\mathbf{M}}_T$ has 3 edges (which is a lower bound for a polygonal shape).

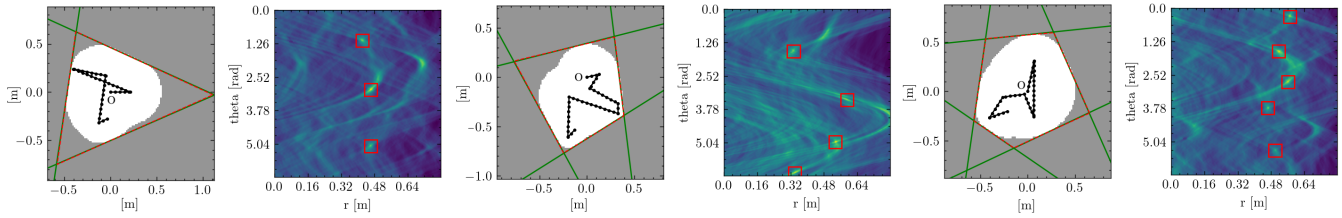

(a) 3 edges geometry (b) 4 edges geometry. (c) 5 edges geometry.

Fig. 2: The different simulated setups along with an instance of mapping results. On the left of each sub-figure, the outline of the ground-truth geometry is provided in discontinuous red, the green lines account for the estimated edges, and the robot path and acquisition positions are represented in black. The corresponding beamforming maps are provided on the right, where the red rectangles indicate the retrieved edges. The edge coordinates are expressed in the fixed frame, whose origin is the initial sensor position O, and the x-axis is aligned with the initial robot heading.

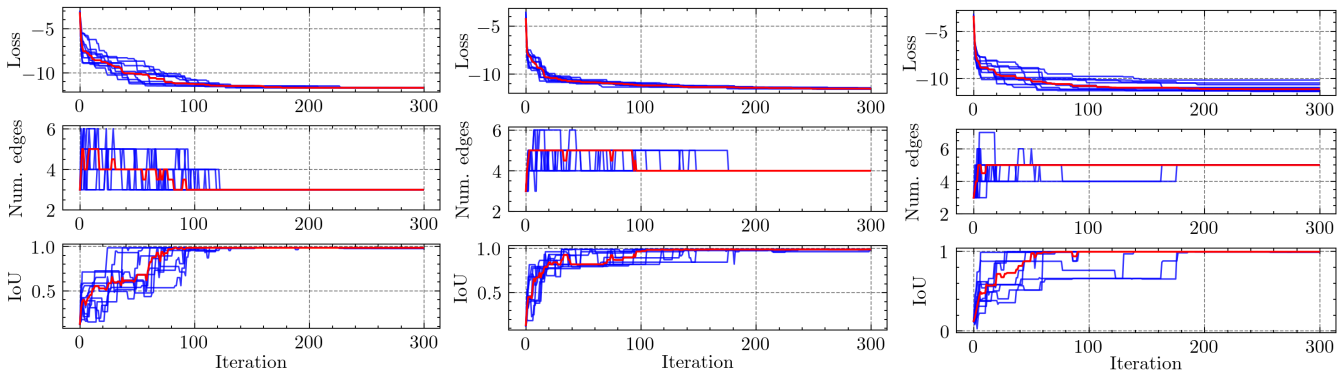

(a) Results for the 3 edges case. (b) Results for the 4 edges case. (c) Results for the 5 edges case.

Fig. 3: Evolution of the performance criteria for the 3 scenarios, and for 10 repetitions of the optimizer. The top plots show, in blue, the evolution of the costs. The middle plots depict the estimated number of edges after application of the edge rejection criterion. The bottom plots show the IoU between estimated and ground-truth surfaces. The median values are in red.

III. Experiments

We perform different experiments to assess the efficiency of our method for recovering arbitrary 2-dimensional polygonal geometries from acoustic echoes acquired over a mobile unit trajectory. We perform simulation tests on three shapes and validation tests using experimental acoustic data acquired on a rectangular metal plate. For this latter scenario, the baseline method in [1] is also applied for comparison.

A. Simulation results

We consider three simulated scenarios, where the geometry to be recovered has either 3, 4 or 5 boundaries. The robot paths are randomly generated with successive linear and rotational displacements. The ultrasonic measurements acquired over the path are simulated using the Image source model and the ultrasonic model g used in [1]. It should be noted that such a data model leads to over-energetic high-order reflections, as acoustic absorption from the boundaries is not taken into account. The excitation $s(t)$ is a two tone bursts sinusoidal wave at 100 kHz. We add Gaussian noise on the measurements to maintain a fixed signal-to-noise ratio SNR $= 0$. The considered geometries and paths are provided in Fig. 2.

We run 10 repetitions of the optimizer for each scenario to assess the repeatability of our approach. The optimizer is set with parameters $\lambda = 3, T(p) = 5/p^{0.8}$, and $V(r,\theta)$ is chosen as the set of edges with line coordinates within the rectangular area centered in (r,θ), and with size 5.4cm × 48 °. Also, we use $K = 10$ as the maximum number of edges. Fig. 3 shows the evolution of the cost, as well as the number of estimated edges after use of the edge rejection criterion during 300 optimizer iterations and for the 10 repetitions. We also display the evolution of $\text{IoU}(\hat{\mathbf{M}}, \mathbf{M})$, which is the IoU between the estimated inner surface (based on the estimated edges) and the ground truth surface $\mathbf{M}$. Hence, an IoU of 1 translates into a perfect geometry estimation. The results demonstrate that, for all the considered scenarios, our approach can seamlessly recover, after convergence, both the actual number of boundaries and the geometric shape.

B. Experimental results

To validate our approach, we run it using experimental ultrasonic data acquired on a rectangular aluminium metal plate by moving, by hand, two nearly collocated contact piezoelectric transducers for emission and reception. More details on the experimental setup and acquisition procedure are provided in [1]. The optimizer is set with the *exact* same parameters than those used for the simulation tests to highlight the robustness of our approach. Also, we do not use ground-

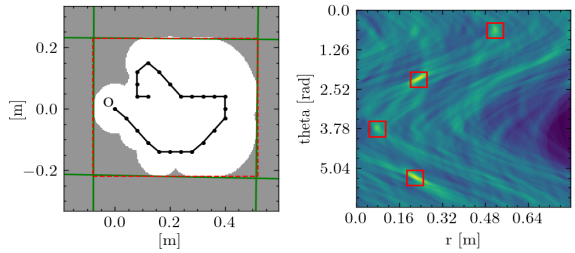

(a) Mapping setup and results for the experimental scenario.

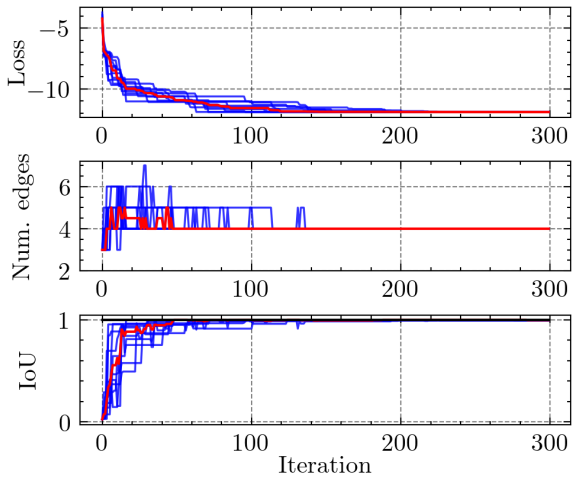

(b) Evolution of performance criteria during the optimization.

Fig. 4: Results for the experimental setup. (a, left) shows the simulated sensor path (in black), the plate outline (red) and estimated edges (green). The corresponding beamforming map is provided on the right, where the red rectangles indicate the retrieved edges. (b) shows the evolution of the loss, the number of estimated edges and IoU for 10 repetitions of the optimizer. The black horizontal line on the IoU plot is the value achieved with the baseline method [1]. The median values are in red.

truth ranges $\rho_{1..T}$, but apply a standard peak detection method on the correlation signals to estimate them. This only leads to a slight estimation error due to high SNR. The considered simulated robot trajectory is depicted in Fig. 4a.

Fig. 4 shows the results and the evolution of the performance criteria for 10 repetitions of the optimization process. For comparison, we also display the IoU achieved with the baseline method presented in [1], which does not require iterative optimization, but is restricted to rectangular shapes. We can see that the estimated number of edges converges seamlessly to 4, while the IoU goes to 1 for all the repetitions. Thus, our method achieves the performance of the baseline approach, despite not being provided with the ground-truth number of edges nor the rectangular constraint. Overall, the results demonstrate the potential of our approach for recovering polygonal shapes from acoustic echoes using a single mobile omnidirectional emitter/receiver device and beamforming.

IV. Conclusion

We have developed a new mapping approach to recover the geometry of unknown 2D polygonal structures from acoustic echos using a single omnidirectional mobile sensor. It combines delay-and-sum beamforming in the geometric boundary space and a simulated annealing optimizer to retrieve boundary estimates from the beamforming results. Contrary to previous works, our approach does not rely on solid hypotheses on echo detection and identification and can recover, in principle, arbitrary polygonal shapes.

The approach is tested in a simulation environment. The results are promising, with a correct and efficient reconstruction of various geometries, without prior knowledge of the number of boundaries to recover. The approach is also validated on experimental acoustic data acquired in a real-life setup to demonstrate its robustness. The results show that the approach achieves the same performance as the baseline method restricted to rectangular geometries. The optimization efficiency shall be improved, in future works, so that the method can be run online. Furthermore, the method shall be integrated within a SLAM framework, as the sensor positions are to be estimated in practice. Its extension to recover 3D volumes shall also be investigated.

References

[1] Ouabi, O. L., Pomarede, P., Geist, M., Declercq, N. F., and Pradalier, C. (2021). A FasSLAM Approach Integrating Beamforming Maps for Ultrasound-based Robotic Inspection of Metal Structures. IEEE Robotics and Automation Letters, 6(2), 2908-2913.

[2] Saqib, U., and Rindom Jensen, J. (2020). A model-based approach to acoustic reflector localization with a robotic platform. IEEE International Conference on Intelligent Robots and Systems, 4499–4504.

[3] Kreković, M., Dokmanić, I., and Vetterli, M. (2016). EchoSLAM: Simultaneous localization and mapping with acoustic echoes. ICASSP, IEEE International Conference on Acoustics, Speech and Signal Processing - Proceedings, 2016-May, 11–15.

[4] Krekovic, M., Dokmanic, I., and Vetterli, M. (2017). Omnidirectional bats, point-to-plane distances, and the price of uniqueness. ICASSP, IEEE International Conference on Acoustics, Speech and Signal Processing - Proceedings, 20, 3261–3265. https://doi.org/10.1109/ICASSP.2017.7952759

[5] Pradalier, C., Ouabi, O. L., Pomarede, P., and Steckel, J. (2020). On-plate localization and mapping for an inspection robot using ultrasonic guided waves: A proof of concept. IEEE International Conference on Intelligent Robots and Systems 5045–5050.

[6] Salvati, D., Drioli, C., and Foresti, G. L. (2016). Sound Source and Microphone Localization from Acoustic Impulse Responses. IEEE Signal Processing Letters, 23(10), 1459–1463.

[7] S. Michaud et al., 3D Localization of a Sound Source Using Mobile Microphone Arrays Referenced by SLAM, 2020 IEEE/RSJ International Conference on Intelligent Robots and Systems (IROS), 2020.

[8] Worley, R., Yu, Y., and Anderson, S. (2020). Acoustic Echo-Localization for Pipe Inspection Robots. IEEE International Conference on Multisensor Fusion and Integration for Intelligent Systems, 2020-Septe, 160–165. https://doi.org/10.1109/MFI49285.2020.9235225

[9] Peng, F., Wang, T., and Chen, B. (2015). Room shape reconstruction with a single mobile acoustic sensor. In 2015 IEEE Global Conference on Signal and Information Processing (GlobalSIP) (pp. 1116-1120).

[10] Van Veen, B. D., and Buckley, K. M. (1988). Beamforming: A versatile approach to spatial filtering. IEEE assp magazine, 5(2), 4-24.

[11] Ouabi, O. L., Pomarede, P., Zeghidour, N., Geist, M., Declercq, N., and Pradalier, C. (2022). Combined Grid and Feature-based Mapping of Metal Structures with Ultrasonic Guided Waves. International Conference on Robotics and Automation 2022, to appear.

[12] Heinrich Kuttruff. Room acoustics. Crc Press, 2016.

[13] Rahman, M. A., and Wang, Y. (2016). Optimizing intersection-over-union in deep neural networks for image segmentation. In International symposium on visual computing (pp. 234-244). Springer, Cham.

[14] Kirkpatrick, S., Gelatt Jr, C. D., and Vecchi, M. P. (1983). Optimization by simulated annealing. science, 220(4598), 671-680.